

A Numerical Study of Wrinkling Evolution of an Elastic Film on a Viscous Layer

Wei Jiang and Zhiping Li*

LMAM & School of mathematical Sciences, Peking University, Beijing 100871, P.R.China

Abstract. The wrinkling phenomenon of a compressed elastic thin film bonded to a viscous layer is studied. Linear stability analysis (LSA) shows that, for materials with cubic crystalline symmetry, the sign of the degree of elastic anisotropy $\zeta = \frac{C_{12}+2C_{44}}{C_{11}} - 1$ plays an important role in the anisotropy of the buckling instability of the thin film system. More precisely, the growth rate of the fastest growing wave number, taking as a function of directions, reaches a peak in the $\langle 100 \rangle$ directions for $\zeta > 0$, and in the $\langle 110 \rangle$ directions for $\zeta < 0$. A highly efficient semi-implicit spectral method is established. The numerical experiments of long time wrinkling evolution processes of a 1+2 dimensional system verified the LSA results, successfully simulated anisotropic wrinkling pattern formation and coarsening, produced a power law scaling and reproduced certain featured phenomena observed in physical experiments.

PACS: 02.70 Hm, 68.08. De, 68.35. Gy, 68.55. -a, 89.75. Da

Key words: wrinkling, anisotropic elastic film, viscous substrate, linear stability analysis, semi-implicit spectral method

1 Introduction

Wrinkling phenomenon at the nanoscale has been simultaneously observed in various thin film systems by many research groups, and attracting ever more attention because of its many important applications, such as stretchable electronics, fabrication based on self-assembly, measuring film elastic properties and many others [1–8]. In general, it is believed that the wrinkled surface is resulted from the compressed residual stress in the thin film, which is produced somehow inevitably in manufacturing processes.

*Corresponding author. *Email address:* lizp@math.pku.edu.cn (Zhiping Li)

The research was supported by the Major State Basic Research Projects (2005CB321701), NSFC projects (10431050 and 10871011) and RFDP of China.

In thin film systems, the film is usually assumed to be made of isotropic or anisotropic elastic materials, while the substrate may be made of elastic, viscous, viscoelastic or plastic materials, the properties of the wrinkling process vary accordingly [9–21]. The study of wrinkling process of an elastic film bonded to a viscous substrate may be traced back to the pioneering work by Hobart and coworkers [1]. They found that a compressively strained heteroepitaxial $Si_{0.7}Ge_{0.3}$ on a low viscosity borophosphosilicate glass layer (BPSG) can lead to surface undulation when annealed at an elevated temperature above the glass transition temperature. By using the atomic force microscopy (AFM) and transmission electron microscopy (TEM), they observed that wrinkles patterns were well organized sinusoids and aligned with the $\langle 100 \rangle$ directions of the cubic crystal $Si_{0.7}Ge_{0.3}$ with a period of about $1\mu m$ and amplitude of about 70–80 nm. Similar experimental observations have been reported by other research groups [22–24]. It is believed that it has important potential applications for designing stress relaxation strategies in semiconductor industries [25, 26].

Many theoretical studies have been inspired by the experiments [9–17]. Earlier studies are mostly focused on the onset of buckling instability of isotropic elastic thin films on viscous substrates [9–12]. By assuming that shear traction at the surface was zero and neglecting the in-plane expansion, Sridhar et al. performed a linear stability analysis (LSA) to determine conditions under which a compressive film on a finite-thickness viscous substrate would buckle and derived the expressions about the critical wave number and the fastest growing wave number of the buckling instability [9]. Coupling both in-plane expansion and wrinkling, Huang and Suo established a system of evolution equations for the wrinkling process, and performed a LSA and numerical simulations for one-dimensional wrinkles of isotropic elastic films [10]. More recently, to analyze the important role played by the anisotropy in the wrinkles pattern formation as is suggested by experimental observations, Im and Huang developed a model for wrinkling evolution process of anisotropic thin films on viscoelastic substrates [17].

While LSA provides crucial information on the initial formation of wrinkles, numerical simulation should be the most convenient tool available to study long time evolution of wrinkling processes. Recently, a 1+1-dimensional (one temporal variable plus one spatial variable) finite difference simulation for the wrinkling process of an isotropic elastic film on a viscous layer has been reported [10, 13].

In the present paper, to further explore the underlying mechanisms of the role played by the anisotropy in the wrinkling evolution process, we generalize Huang-Suo's model [10] to a 1+2-dimensional (one temporal variable plus two spatial variables) mathemat-

ical model for anisotropic elastic thin films with cubic crystalline symmetry, and we apply both the LSA and long time numerical simulations to studying the two-dimensional wrinkles evolution and the scaling law of anisotropic elastic films on viscous layers. It is found that the sign of the degree of the elastic anisotropy $\zeta = \frac{C_{12}+2C_{44}}{C_{11}} - 1$ plays an important role in the anisotropy of the buckling instability of the thin film system. More precisely, we find that, the growth rate of the fastest growing wave number, taking as a function of directions, reaches a peak in the $\langle 100 \rangle$ directions for $\zeta > 0$, and in the $\langle 110 \rangle$ directions for $\zeta < 0$. Numerical experiments of long time wrinkling evolution processes verified the LSA results, successfully simulated anisotropic wrinkling pattern formation and coarsening, produced a power law scaling and reproduced certain featured phenomena observed in physical experiments. Both the analytical and numerical results are qualitatively in accordance with the physical experiments recently done by several research groups [1,22–24].

The rest of the paper is organized as follows. In Section 2, we briefly present the classical Föppl-von Karman(FvK) theory for thin elastic plates with cubic crystalline symmetry, and derive governing equations for the wrinkling evolution process for an anisotropic thin film system. In Section 3, a LSA is performed to reveal how the elastic anisotropy affects the initial buckling of the thin film. A highly efficient numerical algorithm, based on a semi-implicit spectral method making fully use of fast Fourier transform(FFT), is developed for the 1+2-dimensional wrinkling evolution process in Section 4. Numerical results are presented and discussed in Section 5. Finally, Section 6 concludes the paper with a summary.

2 Model formulation

In this section, the governing equations for anisotropic elastic thin films on viscous layers are derived. Similar to the approach in [17], we adopt the anisotropic FvK theory to describe the deformation of anisotropic elastic thin films. The significant difference is that, instead of a compressible viscoelastic layer considered in [17], we consider the substrate layer as an incompressible viscous layer. The difference will lead to quite different evolution process and thus power laws for coarsening.

Suppose that an elastic thin film with thickness h is bonded to a viscous layer with thickness H , which in turn is bonded to a rigid substrate. At the reference state, the film is assumed to be flat. To relax the strain energy caused by the intensive compressive residual stress, the elastic thin film will deform with in-plane expansion and out-of-plane

wrinkling with certain preferred pattern and scale, as is illustrated schematically in Figure 1. At the same time, the traction force generated by the deformation of the elastic thin film will drive the viscous layer to flow and further dissipate the energy of the system. The elastic thin film and the viscous layer are supposed to be strictly bonded to each other, thus the elastic film will never delaminate from the viscous layer during the wrinkling evolution process. We assume that the motion of the elastic film is quasi-static, i.e. the inertia force is neglected.

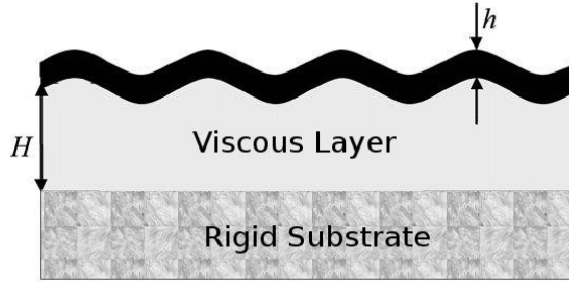


FIGURE 1: Wrinkling of an elastic film on a viscous layer

2.1 Deformation of the thin film

Because the magnitude of out-of-plane displacement has the same order as that of the thickness of thin film layer during the deformation, the Föppl-von Karman large deflection plate theory is adopted to describe the deformation of the thin film layer. We suppose that the thin film layer is a homogeneous linear elastic plate which has cubic crystalline symmetry with three independent elastic stiffness constants C_{11} , C_{12} and C_{44} , and the surface of the plate coincides with the (001) crystal plane, and the Cartesian coordinate system (x_1^*, x_2^*, x_3^*) is taken in accordance with the cubic edges of the crystal unit cell.

Let Ω and $B = \Omega \times [-\frac{h}{2}, \frac{h}{2}]$ be the reference configurations of a 2-dimensional surface (say the middle surface) and the 3-dimensional body of the plate respectively. For convenience, we will use the asterisk and prime as superscripts to distinguish the physical quantities defined on Ω and B . Especially, we denote (u_1^*, u_2^*) and (u_1', u_2') the in-plane displacements along x_1^* and x_2^* directions, w^* and w' the out-of-plane displacements, $\epsilon_{\alpha\beta}^*$ and $\epsilon'_{\alpha\beta}$ the strain tensors, $\sigma_{\alpha\beta}^*$ and $\sigma'_{\alpha\beta}$ the stress tensors, which are considered to be defined on Ω and B respectively.

To establish the governing equations for the deformation of the thin film, we recall

the following underlying hypotheses for deriving FvK equations [27,28]:

- (i) Direct normal lines assumption: a normal line to the mid-surface of the plate before deformation remains a normal line to the deformed mid-surface. Under such an assumption, the transverse shear stresses are thus neglected.
- (ii) The normal stress along the transverse direction is small compared with the other stresses, and is also neglected.
- (iii) A nonlinear strain-displacement relations is used by neglecting the high order non-linear terms produced by in-plane displacements.

Under the assumption (iii) and due to the existence of initial residual stress, the strain $\epsilon'_{\alpha\beta}$ in the thin film can be expressed as

$$\epsilon'_{\alpha\beta} = \frac{1}{2} \left(\frac{\partial u'_\alpha}{\partial x^*_\beta} + \frac{\partial u'_\beta}{\partial x^*_\alpha} + \frac{\partial w'}{\partial x^*_\alpha} \frac{\partial w'}{\partial x^*_\beta} \right) + \epsilon^o_{\alpha\beta}. \quad (2.1)$$

where $\epsilon^o_{\alpha\beta}$ is the initial residual strain tensor. If the residual strain is equi-biaxial, we can express that $\epsilon^o_{\alpha\beta} = \epsilon^o \delta_{\alpha\beta}$, where $\delta_{\alpha\beta}$ is the Kronecker delta, and ϵ^o is the magnitude of the equi-biaxial residual strain. If $\epsilon^o > 0$, it means that the residual strain is tensile; while if $\epsilon^o < 0$, it corresponds to compressive residual strain. It is assumed that the initial residual strain is compressive in this paper. Accordingly, the initial residual stress tensor $\sigma^o_{\alpha\beta}$ can be defined corresponding to $\epsilon^o_{\alpha\beta}$. The Greek subscripts α and β run from 1 to 2.

By the assumption (i), we can easily represent the displacements u'_α, w' with the middle surface displacements u^*_α and w^* as follows:

$$u'_\alpha = u^*_\alpha - x^*_3 \frac{\partial w^*}{\partial x^*_\alpha}, \quad (2.2)$$

$$w' = w^*. \quad (2.3)$$

Inserting the eqs. (2.2) and (2.3) into the strain-displacement relations (2.1), we can express the strain tensor defined on the whole plate by that defined on the middle surface of the plate:

$$\epsilon'_{\alpha\beta} = \epsilon^*_{\alpha\beta} - x^*_3 \frac{\partial^2 w^*}{\partial x^*_\alpha \partial x^*_\beta}. \quad (2.4)$$

Because the thin film material has the cubic crystalline symmetry, according to the linear elasticity theory, the constitutive equation can be expressed with three independent elastic constants by the generalized Hooke's law [30]

$$\begin{pmatrix} \sigma'_{11} \\ \sigma'_{22} \\ \sigma'_{33} \\ \sigma'_{13} \\ \sigma'_{23} \\ \sigma'_{12} \end{pmatrix} = \begin{pmatrix} C_{11} & C_{12} & C_{12} & 0 & 0 & 0 \\ C_{12} & C_{11} & C_{12} & 0 & 0 & 0 \\ C_{12} & C_{12} & C_{11} & 0 & 0 & 0 \\ 0 & 0 & 0 & 2C_{44} & 0 & 0 \\ 0 & 0 & 0 & 0 & 2C_{44} & 0 \\ 0 & 0 & 0 & 0 & 0 & 2C_{44} \end{pmatrix} \begin{pmatrix} \epsilon'_{11} \\ \epsilon'_{22} \\ \epsilon'_{33} \\ \epsilon'_{13} \\ \epsilon'_{23} \\ \epsilon'_{12} \end{pmatrix}. \quad (2.5)$$

However, according to the hypotheses (i) and (ii), the whole plate is under the plane stress state, i.e. $\sigma'_{13} = \sigma'_{23} = \sigma'_{33} = 0$. This leads to a compact constitutive equation

$$\begin{pmatrix} \sigma'_{11} \\ \sigma'_{22} \\ \sigma'_{12} \end{pmatrix} = \begin{pmatrix} \bar{C}_{11} & \bar{C}_{12} & 0 \\ \bar{C}_{12} & \bar{C}_{11} & 0 \\ 0 & 0 & 2C_{44} \end{pmatrix} \begin{pmatrix} \epsilon'_{11} \\ \epsilon'_{22} \\ \epsilon'_{12} \end{pmatrix}, \quad (2.6)$$

where $\bar{C}_{11} = C_{11} - \frac{C_{12}^2}{C_{11}}$, $\bar{C}_{12} = C_{12} - \frac{C_{12}^2}{C_{11}}$. In the isotropic case when $2C_{44} = C_{11} - C_{12}$, $\bar{C}_{11} = \frac{E}{1-\nu^2}$, $\bar{C}_{12} = \frac{E\nu}{1-\nu^2}$, where E is the Young modulus and ν is the Poisson ratio.

Due to the elastic deformation, the elastic thin film stores the elastic strain energy W_E , which can be expressed as

$$\begin{aligned} W_E &= \iiint_B \frac{1}{2} \left(\sigma'_{11} \epsilon'_{11} + \sigma'_{22} \epsilon'_{22} + 2\sigma'_{12} \epsilon'_{12} \right) dx_1^* dx_2^* dx_3^* \\ &= \iint_{\Omega} \int_{[-\frac{h}{2}, \frac{h}{2}]} \frac{1}{2} \left(\sigma'_{11} \epsilon'_{11} + \sigma'_{22} \epsilon'_{22} + 2\sigma'_{12} \epsilon'_{12} \right) dx_3^* dx_1^* dx_2^*. \end{aligned} \quad (2.7)$$

Substituting equation (2.6) together with equation (2.4) into equation (2.7), and integrating with respect to x_3^* over the thickness of the thin film layer, we obtain

$$W_E = \iint_{\Omega} \left(E^m + E^b \right) dx_1^* dx_2^*, \quad (2.8)$$

where in (2.8)

$$E^m = \frac{1}{2} \left(N_{11}^* \epsilon_{11}^* + N_{22}^* \epsilon_{22}^* + 2N_{12}^* \epsilon_{12}^* \right) \quad (2.9)$$

is the membrane strain energy density with

$$N_{\alpha\beta}^* = \int_{-\frac{h}{2}}^{\frac{h}{2}} \sigma'_{\alpha\beta} dx_3^* \quad (2.10)$$

being the membrane stress tensor, and where in (2.8)

$$E^b = \frac{1}{2} \left(B_{11}^* \chi_{11}^* + B_{22}^* \chi_{22}^* + 2B_{12}^* \chi_{12}^* \right), \quad (2.11)$$

is the bending moment energy density with

$$B_{\alpha\beta}^* = - \int_{-\frac{h}{2}}^{\frac{h}{2}} \sigma'_{\alpha\beta} x_3^* dx_3^*, \quad (2.12)$$

$$\chi_{\alpha\beta}^* = \frac{\partial^2 w^*}{\partial x_\alpha^* \partial x_\beta^*}. \quad (2.13)$$

being the bending moment and strain tensor respectively.

Denote q^* and τ_1^*, τ_2^* the normal and shear traction forces that the viscous layer exerts on the thin elastic film, then the virtue work done by the forces can be expressed as

$$\delta W_F = \iint_{\Omega} (q^* \delta w^* + \tau_1^* \delta u_1^* + \tau_2^* \delta u_2^*) dx_1^* dx_2^*. \quad (2.14)$$

Since it is assumed that the motion of the thin elastic film is quasi-static, the principle of virtue work states

$$\delta W_E = \delta W_F, \quad (2.15)$$

which leads to the following relations:

$$q^* = \frac{h^3}{12} \left[\bar{C}_{11} \frac{\partial^4 w^*}{\partial (x_1^*)^4} + 2(\bar{C}_{12} + 2C_{44}) \frac{\partial^4 w^*}{\partial (x_1^*)^2 \partial (x_2^*)^2} + \bar{C}_{11} \frac{\partial^4 w^*}{\partial (x_2^*)^4} \right] - h \frac{\partial}{\partial x_\alpha^*} \left(\sigma_{\alpha\beta}^* \frac{\partial w^*}{\partial x_\beta^*} \right), \quad (2.16)$$

$$\tau_\alpha^* = -h \frac{\partial \sigma_{\alpha\beta}^*}{\partial x_\beta^*}, \quad (2.17)$$

where $\sigma_{\alpha\beta}^*$ is the stress tensor defined on the middle surface of the film through (2.4) and (2.6), and the repeated Greek subscripts α, β stand for summation over $\alpha, \beta = 1, 2$.

2.2 Flow of the viscous layer

According to the law of action and reaction, the glass layer (BPSG) is subjected to the normal and shear traction forces $-q^*$ and $-\tau_1^*, -\tau_2^*$ exerted by the elastic thin film through their contact interface, which will drive the substance to creep between the two nearly parallel surfaces when the temperature is raised up to above the glass transition temperature. Suppose that the motion is so slow that the inertial term can be ignored, then the flow described by the incompressible Navier-Stokes equations reduces to the so called Stokes flow or Creeping flow. Suppose further that, (1) the out-of-plane displacement is much smaller than the thickness H of the viscous layer, i.e. $w^* \ll H$; (2) H is small as compared with the characteristic lengths, such as the wrinkling wavelengths, in the x_1^* and x_2^* directions; (3) the in-plane derivatives of the in-plane velocity are negligible as compared with its normal derivative, which is often considered as a natural consequence of (2). Under such assumptions, following the approach by Huang and Suo [10], the Reynolds lubrication theory [31] on viscous creeping flow can be applied to further reduce the governing equations and the velocities $\frac{\partial w^*}{\partial t^*}, \frac{\partial u_1^*}{\partial t^*}, \frac{\partial u_2^*}{\partial t^*}$ on the interface can be expressed as

$$\frac{\partial w^*}{\partial t^*} = \frac{\partial}{\partial x_\alpha^*} \left(\frac{H^3}{3\eta} \frac{\partial q^*}{\partial x_\alpha^*} + \frac{H^2}{2\eta} \tau_\alpha^* \right), \quad (2.18)$$

$$\frac{\partial u_\alpha^*}{\partial t^*} = -\frac{H^2}{2\eta} \frac{\partial q^*}{\partial x_\alpha^*} - \frac{H}{\eta} \tau_\alpha^*, \quad \alpha = 1, 2, \quad (2.19)$$

where η is the viscosity of the glass layer. We will see that, at least for the initial growth stage, the assumptions (1)–(3) are well satisfied; while for the coarsening stage, the approximation might be problematic. Notice that the terms q^*, τ_1^*, τ_2^* in eqs. (2.18)–(2.19) are given by (2.16) and (2.17), these form a system of partial differential equations (PDEs) for the the temporal-spatial wrinkling evolution process.

2.3 Dimensionless

For the convenience of further discussions, we perform the following changes of variables: the lengths, stress and time variables are respectively normalized by h, C_{11} and

$\frac{\eta}{C_{11}}$, i.e.

$$\begin{pmatrix} x_1^* \\ x_2^* \end{pmatrix} = h \begin{pmatrix} x_1 \\ x_2 \end{pmatrix}, \quad \begin{pmatrix} u_1^* \\ u_2^* \\ w^* \end{pmatrix} = h \begin{pmatrix} u_1 \\ u_2 \\ w \end{pmatrix}, \quad (2.20)$$

$$\begin{pmatrix} q^* \\ \tau_1^* \\ \tau_2^* \end{pmatrix} = C_{11} \begin{pmatrix} q \\ \tau_1 \\ \tau_2 \end{pmatrix}, \quad \sigma_{\alpha\beta}^* = C_{11} \sigma_{\alpha\beta}, \quad (2.21)$$

$$t^* = \frac{\eta}{C_{11}} t. \quad (2.22)$$

With the above set of non-dimensional variables, a complete system of non-dimensional temporal-spatial PDEs for the wrinkling evolution of anisotropic elastic thin films on viscous substrates can be expressed as

$$\frac{\partial w}{\partial t} = \frac{\partial}{\partial x_\alpha} \left(\frac{1}{3} h_r^3 \frac{\partial q}{\partial x_\alpha} + \frac{1}{2} h_r^2 \tau_\alpha \right), \quad (2.23)$$

$$\frac{\partial u_\alpha}{\partial t} = -\frac{1}{2} h_r^2 \frac{\partial q}{\partial x_\alpha} - h_r \tau_\alpha, \quad (2.24)$$

where $h_r = \frac{H}{h}$ is the thickness ratio, and

$$q = \frac{1}{12} \left[\widehat{C}_{11} \frac{\partial^4 w}{\partial x_1^4} + 2(\widehat{C}_{12} + 2\widehat{C}_{44}) \frac{\partial^4 w}{\partial x_1^2 \partial x_2^2} + \widehat{C}_{11} \frac{\partial^4 w}{\partial x_2^4} \right] - \frac{\partial}{\partial x_\alpha} \left(\sigma_{\alpha\beta} \frac{\partial w}{\partial x_\beta} \right), \quad (2.25)$$

$$\tau_\alpha = -\frac{\partial \sigma_{\alpha\beta}}{\partial x_\beta}, \quad (2.26)$$

where $\widehat{C}_{11} = \overline{C}_{11}/C_{11}$, $\widehat{C}_{12} = \overline{C}_{12}/C_{11}$, $\widehat{C}_{44} = C_{44}/C_{11}$ are the normalized elastic constants. In the rest of the paper, we concentrate on the solution of the PDEs system (2.23)-(2.26), hence all of the physical variables involved are normalized and dimensionless.

3 Linear stability analysis

It is easily verified that the reference state, $w = u_1 = u_2 = 0$, is a trivial solution to the coupled evolution equations (2.23)-(2.26). Since the thin film is supposed to be initially flat and subjected to a uniform compressive residual stress $\sigma_{\alpha\beta}^0$, the reference state may

be unstable and the film may buckle to relax the strain energy. We consider a small perturbation of the reference state of the form:

$$w(x_1, x_2) = A_1(t) \cos[k(x_1 \cos \theta + x_2 \sin \theta)], \quad (3.1)$$

$$u_1(x_1, x_2) = A_2(t) \sin[k(x_1 \cos \theta + x_2 \sin \theta)], \quad (3.2)$$

$$u_2(x_1, x_2) = A_3(t) \sin[k(x_1 \cos \theta + x_2 \sin \theta)], \quad (3.3)$$

where k is a wave number, θ is an angle of the wave vector, which is measured from the x_1 axis or the [100] axis of the cubic crystal film, and A_1, A_2, A_3 are respectively a function of time and represent the amplitudes of the displacements.

Substituting eqs. (3.1)-(3.3) into eqs. (2.23)-(2.26) and retaining the first order terms, we obtain the following system of ordinary differential equations (ODEs):

$$\frac{d}{dt} \begin{pmatrix} A_1 \\ A_2 \\ A_3 \end{pmatrix} = M \begin{pmatrix} A_1 \\ A_2 \\ A_3 \end{pmatrix}, \quad (3.4)$$

where $M = (M_{ij})_{1 \leq i, j \leq 3}$ is a 3×3 matrix given by

$$M = \begin{bmatrix} -\frac{1}{3}h_r^3(\frac{1}{12}k^6 E_\theta + k^4 \sigma_\theta) & \frac{1}{2}h_r^2 k^3 D_1 \cos \theta & \frac{1}{2}h_r^2 k^3 D_2 \sin \theta \\ \frac{1}{2}h_r^2(\frac{1}{12}k^5 E_\theta + k^3 \sigma_\theta) \cos \theta & -h_r k^2(\widehat{C}_{11} \cos^2 \theta + \widehat{C}_{44} \sin^2 \theta) & -h_r k^2(\widehat{C}_{12} + \widehat{C}_{44}) \sin \theta \cos \theta \\ \frac{1}{2}h_r^2(\frac{1}{12}k^5 E_\theta + k^3 \sigma_\theta) \sin \theta & -h_r k^2(\widehat{C}_{12} + \widehat{C}_{44}) \sin \theta \cos \theta & -h_r k^2(\widehat{C}_{11} \sin^2 \theta + \widehat{C}_{44} \cos^2 \theta) \end{bmatrix}$$

with

$$E_\theta = \widehat{C}_{11} \cos^4 \theta + \widehat{C}_{11} \sin^4 \theta + 2(\widehat{C}_{12} + 2\widehat{C}_{44}) \sin^2 \theta \cos^2 \theta,$$

$$\sigma_\theta = \widehat{\sigma}_{11}^o \cos^2 \theta + \widehat{\sigma}_{22}^o \sin^2 \theta + 2\widehat{\sigma}_{12}^o \sin \theta \cos \theta,$$

$$D_1 = \widehat{C}_{11} \cos^2 \theta + (\widehat{C}_{12} + 2\widehat{C}_{44}) \sin^2 \theta,$$

$$D_2 = \widehat{C}_{11} \sin^2 \theta + (\widehat{C}_{12} + 2\widehat{C}_{44}) \cos^2 \theta.$$

where $\widehat{\sigma}_{\alpha\beta}^o$ is the normalized initial residual stress, i.e. $\widehat{\sigma}_{\alpha\beta}^o = \frac{\sigma_{\alpha\beta}^o}{\widehat{C}_{11}}$.

The solution of the system (3.4) takes the following form:

$$A_i(t) = \sum_{j=1}^3 B_{ij} e^{\lambda_j t}, \quad i = 1, 2, 3, \quad (3.5)$$

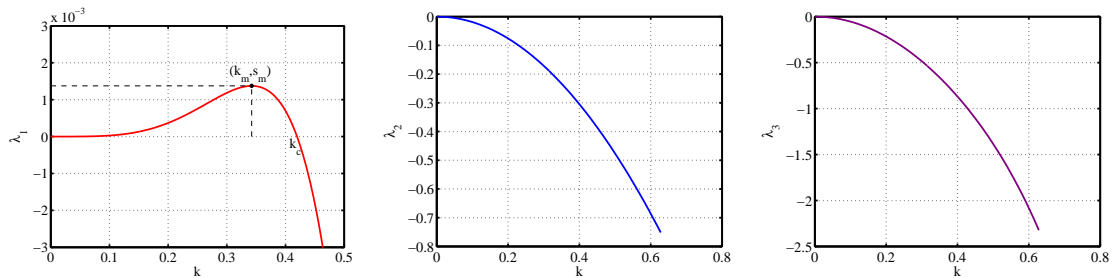


FIGURE 2: A typical numerical result of the eigenvalues of the matrix M as functions of the wave number.

where $\lambda_1, \lambda_2, \lambda_3$ are the three eigenvalues of the matrix M , and the coefficients B_{ij} are determined by the initial data. Therefore, basically, the stability of the corresponding solutions of the system is determined by the signs of the real part of the eigenvalues.

Our numerical experiments on the thin film systems, which are made of typical elastic materials with the cubic crystalline symmetry and subjected to uniform equi-biaxial compressive residual stresses, show that, the three eigenvalues of M are always real; and if ordered as $\lambda_1 \geq \lambda_2 \geq \lambda_3$, then, λ_2 and λ_3 are always negative and are decreasing functions with respect to the wave number k , and there is a critical wave number $k_c > 0$ such that, λ_1 is negative for all $k > k_c$, and is positive for all $0 < k < k_c$; furthermore, there is a fastest growing wave number $k_m \in (0, k_c)$, such that λ_1 is strictly increasing with respect to k for $k < k_m$ and strictly decreasing with respect to k for $k > k_m$, and consequently λ_1 reaches the unique maximum value s_m at $k = k_m$. A typical numerical result is shown in Figure 2.

TABLE 1: Elastic constants for three different cubic crystals [17, 30]

Crystal	C_{11} (GPa)	C_{12} (GPa)	C_{44} (GPa)	Degree of anisotropic ζ
$Si_{0.7}Ge_{0.3}$	154.9	59.5	75.9	0.36
Cr	339.8	58.6	99.0	-0.24
Isotropic (Supposed)	161.7	69.3	46.2	0.00

Table 1 shows the elastic constants of three different cubic crystalline materials which we used in our numerical experiments, where $\zeta = \frac{C_{12} + 2C_{44}}{C_{11}} - 1$ characterizes the degree of elastic anisotropy. It is easy to verify that on the (001) crystal plane, the elastic stiffness is minimized in $\langle 100 \rangle$ crystallographic directions ($\theta = 0, \frac{\pi}{2}$) when $\zeta > 0$; while it is minimized in $\langle 110 \rangle$ directions ($\theta = \frac{\pi}{4}, \frac{3\pi}{4}$) when $\zeta < 0$; and the material is isotropic when $\zeta = 0$, and in such a case, the stiffness is independent of the direction [29, 30]. Intuitively

speaking, the buckling instability should most likely be observed in the softest directions. This is in fact further confirmed by our numerical experiments.

In the isotropic case when $\zeta = \frac{C_{12}+2C_{44}}{C_{11}} - 1 = 0$, if the film is subjected to uniform equibiaxial compressive residual stress (i.e. $\hat{\sigma}_{\alpha\beta}^o = \sigma^o \delta_{\alpha\beta}$), a direct calculation shows that the three eigenvalues of the matrix M are independent of the wave vector θ . Therefore, the growth rate is independent of crystallographic directions. For an isotropic material with elastic constants shown in Table 1, which has corresponding Young modulus $E = 123.2$ GPa and Poisson ratio $\nu = 0.33$, the numerical results on the growth rates are shown in Figure 3 and Figure 4. It is clearly seen in the figures that the fastest growth rate s_m is an increasing function of both the magnitude of residual stress $|\sigma^o|$ and the thickness ratio h_r , on the other hand, the fastest growing wave number k_m and the critical wave number k_c are increasing functions of the $|\sigma^o|$, while the critical wave number k_c is independent of the h_r . The numerical results are consistent with the analysis conducted by other researchers [9–11].

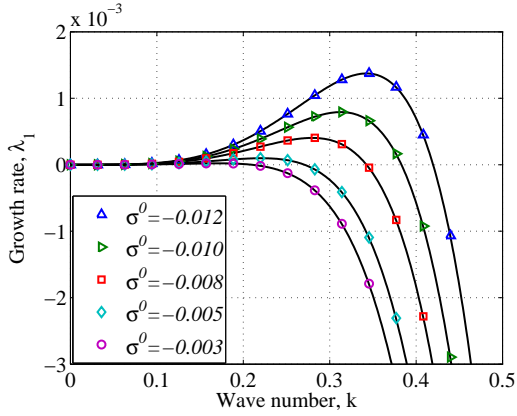


FIGURE 3: The growth rate as a function of wave number for various equi-biaxial compressive residual stresses with fixed thickness ratio $h_r = \frac{20}{3}$.

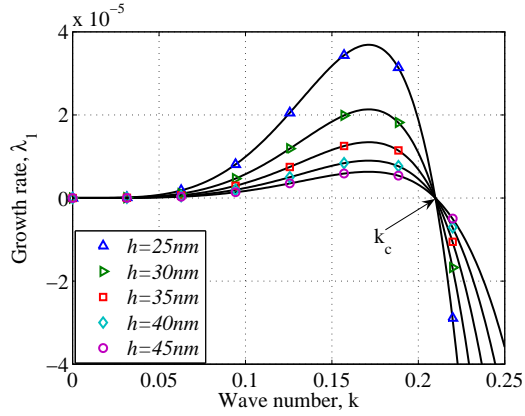


FIGURE 4: The growth rate as a function of wave number for various thickness ratios $h_r = \frac{H}{h}$, where $H = 200\text{nm}$ and $\sigma^o = -0.003$ are fixed.

In the anisotropic case, we choose two typical cubic crystal materials for the numerical experiments, one is the crystal $Si_{0.7}Ge_{0.3}$ for which the degree of anisotropic $\zeta > 0$; the other is the crystal Cr for which $\zeta < 0$. Figure 5 shows the numerical results on the growth rate for the cubic crystal $Si_{0.7}Ge_{0.3}$ film as a function of wave number for various wave vectors. It shows that the fastest growth rate s_m attains the maximum in $\langle 100 \rangle$ crystallographic directions ($\theta = 0, \frac{\pi}{2}$) and the minimum in $\langle 110 \rangle$ crystallographic directions ($\theta = \frac{\pi}{4}, \frac{3\pi}{4}$). While for the crystal Cr , the trend is just opposite as is revealed

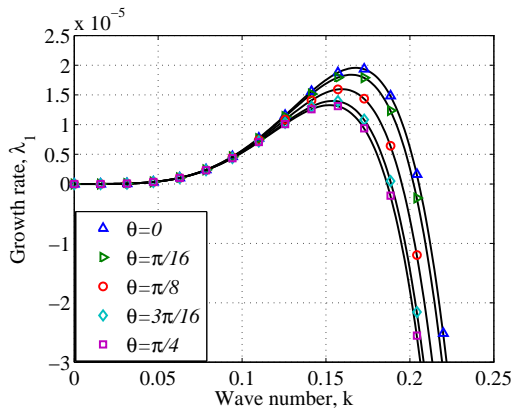


FIGURE 5: The growth rate for the cubic crystal $Si_{0.7}Ge_{0.3}$ film with $\zeta > 0$ as a function of wave number for various wave vectors, where $\sigma^o = -0.003$ and $h_r = \frac{20}{3}$.

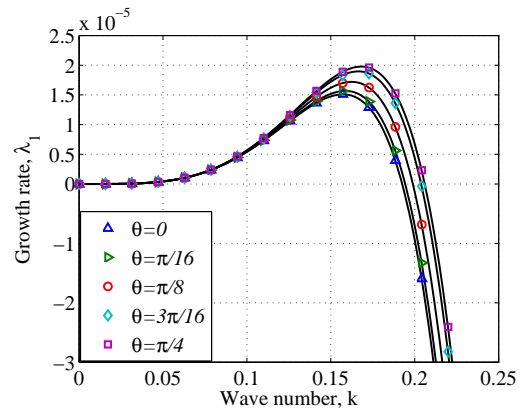


FIGURE 6: The growth rate for the cubic crystal Cr film with $\zeta < 0$ as a function of wave number for various wave vectors, where $\sigma^o = -0.003$ and $h_r = \frac{20}{3}$.

by the numerical results shown in Figure 6. The LSA indicates that the fastest growing wavelengths along different directions are different, however the perturbation wavelength most likely to be observed in the real experiments should be the one with the maximum fastest growth rate. This observation is in agreement with our subsequent numerical experiments.

4 Numerical algorithm for long time evolution

While the LSA provides valuable insight into the early stage of wrinkling evolution, to study the wrinkling patterns and scaling laws the instability may lead to in a long run, we need to work on other approaches, such as numerical simulations. The partial differential equations (2.23)–(2.26) are coupled highly nonlinear sixth order PDEs. To apply explicit finite difference schemes to such a system, the typical stability requirement on the time step is $\Delta t < c(\Delta x)^6$ for some problem dependent constant c , which is obviously too strict for long time numerical simulations. On the other hand, the implicit finite difference schemes, such as Crank-Nicolson type schemes, usually do have much relaxed restrictions on the time step, however, since a system of nonlinear algebraic equations must be solved numerically in each time step, the total cost of a long time numerical simulation can still be too much a burden. Inspired by the semi-implicit spectral methods proposed by Chen and shen [32], we developed an efficient algorithm for the system (2.23)–(2.26), which turned out to be stable for reasonably big time steps and sufficiently accurate for

our purpose. The basic idea is that, we first transform the system of the PDEs into a system of ODEs by means of the Fourier transform, and then apply a semi-implicit numerical scheme to solve the deduced ODE system, where the nonlinear terms are treated explicitly and computed by using as much FFT as possible. The development of the algorithm is sketched as follows.

Denote $\mathcal{F}[\phi] = \int_{-\infty}^{\infty} \int_{-\infty}^{\infty} \phi(x_1, x_2, t) e^{-i(k_1 x_1 + k_2 x_2)} dx_1 dx_2$ the Fourier transform of a given

function $\phi(x_1, x_2, t)$, where k_1 and k_2 are the variables in the Fourier space and $i = \sqrt{-1}$. By performing the Fourier transform on the both sides of Eqs. (2.23) and (2.24) with q and τ giving by (2.25) and (2.26), regarding the Fourier space variables k_1 and k_2 as parameters, we obtain a system of ODEs:

$$\frac{\partial \mathcal{F}[w]}{\partial t} = L_{11} \mathcal{F}[w] + L_{12} \mathcal{F}[u_1] + L_{13} \mathcal{F}[u_2] + NL_1, \quad (4.1)$$

$$\frac{\partial \mathcal{F}[u_1]}{\partial t} = L_{21} \mathcal{F}[w] + L_{22} \mathcal{F}[u_1] + L_{23} \mathcal{F}[u_2] + NL_2, \quad (4.2)$$

$$\frac{\partial \mathcal{F}[u_2]}{\partial t} = L_{31} \mathcal{F}[w] + L_{32} \mathcal{F}[u_1] + L_{33} \mathcal{F}[u_2] + NL_3, \quad (4.3)$$

where

$$L_{11} = -\frac{h_r^3}{36} [\widehat{C}_{11}(k_1^4 + k_2^4) + 2(\widehat{C}_{12} + 2\widehat{C}_{44})k_1^2 k_2^2] k^2,$$

$$L_{12} = i \frac{h_r^2}{2} [\widehat{C}_{11} k_1^3 + (\widehat{C}_{12} + 2\widehat{C}_{44}) k_1 k_2^2], \quad L_{13} = i \frac{h_r^2}{2} [\widehat{C}_{11} k_2^3 + (\widehat{C}_{12} + 2\widehat{C}_{44}) k_1^2 k_2],$$

$$NL_1 = \frac{h_r^2}{2} k_\alpha k_\beta \mathcal{F}[Q_{\alpha\beta}] + i \frac{h_r^3}{3} k^2 k_\alpha \mathcal{F}[M_\alpha],$$

$$L_{21} = -i \frac{h_r^2}{24} k_1 [\widehat{C}_{11}(k_1^4 + k_2^4) + 2(\widehat{C}_{12} + 2\widehat{C}_{44})k_1^2 k_2^2],$$

$$L_{22} = -h_r (\widehat{C}_{11} k_1^2 + \widehat{C}_{44} k_2^2), \quad L_{23} = -h_r (\widehat{C}_{12} + \widehat{C}_{44}) k_1 k_2,$$

$$NL_2 = -\frac{h_r^2}{2} k_1 k_\alpha \mathcal{F}[M_\alpha] + i h_r k_\alpha \mathcal{F}[Q_{\alpha 1}],$$

$$L_{31} = -i \frac{h_r^2}{24} k_2 [\widehat{C}_{11}(k_1^4 + k_2^4) + 2(\widehat{C}_{12} + 2\widehat{C}_{44})k_1^2 k_2^2],$$

$$L_{32} = L_{23}, \quad L_{33} = -h_r (\widehat{C}_{11} k_2^2 + \widehat{C}_{44} k_1^2),$$

$$NL_3 = -\frac{h_r^2}{2} k_2 k_\alpha \mathcal{F}[M_\alpha] + i h_r k_\alpha \mathcal{F}[Q_{\alpha 2}].$$

and where $k = \sqrt{k_1^2 + k_2^2}$, $Q_{\alpha\beta}$ is a symmetric tensor defined as

$$\begin{pmatrix} Q_{11} \\ Q_{22} \\ Q_{12} \end{pmatrix} = \frac{1}{2} \begin{pmatrix} \hat{C}_{11} & \hat{C}_{12} & 0 \\ \hat{C}_{12} & \hat{C}_{11} & 0 \\ 0 & 0 & 2\hat{C}_{44} \end{pmatrix} \begin{pmatrix} \left(\frac{\partial w}{\partial x_1}\right)^2 \\ \left(\frac{\partial w}{\partial x_2}\right)^2 \\ \frac{\partial w}{\partial x_1} \frac{\partial w}{\partial x_2} \end{pmatrix},$$

and

$$M_\alpha = \sigma_{\alpha\beta} \frac{\partial w}{\partial x_\beta} = (\hat{\sigma}_{\alpha\beta}^o + \tilde{\sigma}_{\alpha\beta}) \frac{\partial w}{\partial x_\beta},$$

where $\sigma_{\alpha\beta}$ is the normalized total stress in the thin film, which includes two parts: one is the normalized initial residual stress $\hat{\sigma}_{\alpha\beta}^o$, and the other is the additional stress $\tilde{\sigma}_{\alpha\beta}$ produced by the buckling deformation of the thin film.

Suppose the problem is periodic with respect to the spatial variables x_1 and x_2 , then, by performing the corresponding discrete Fourier transforms, we obtain a finite system of ODEs of the form (4.1)-(4.3). To fully discretize the problem, we apply the following semi-implicit numerical scheme

$$\frac{\mathcal{F}[w]^{n+1} - \mathcal{F}[w]^n}{\Delta t} = L_{11}\mathcal{F}[w]^{n+1} + L_{12}\mathcal{F}[u_1]^{n+1} + L_{13}\mathcal{F}[u_2]^{n+1} + NL_1^n, \quad (4.4)$$

$$\frac{\mathcal{F}[u_1]^{n+1} - \mathcal{F}[u_1]^n}{\Delta t} = L_{21}\mathcal{F}[w]^{n+1} + L_{22}\mathcal{F}[u_1]^{n+1} + L_{23}\mathcal{F}[u_2]^{n+1} + NL_2^n, \quad (4.5)$$

$$\frac{\mathcal{F}[u_2]^{n+1} - \mathcal{F}[u_2]^n}{\Delta t} = L_{31}\mathcal{F}[w]^{n+1} + L_{32}\mathcal{F}[u_1]^{n+1} + L_{33}\mathcal{F}[u_2]^{n+1} + NL_3^n, \quad (4.6)$$

where the linear terms are treated implicitly, while the nonlinear terms are treated explicitly. The equations (4.4)-(4.6) can be equivalently written in the following matrix form:

$$\begin{bmatrix} 1 - L_{11}\Delta t & -L_{12}\Delta t & -L_{13}\Delta t \\ -L_{21}\Delta t & 1 - L_{22}\Delta t & -L_{23}\Delta t \\ -L_{31}\Delta t & -L_{32}\Delta t & 1 - L_{33}\Delta t \end{bmatrix} \begin{bmatrix} \mathcal{F}[w]^{n+1} \\ \mathcal{F}[u_1]^{n+1} \\ \mathcal{F}[u_2]^{n+1} \end{bmatrix} = \begin{bmatrix} \mathcal{F}[w]^n \\ \mathcal{F}[u_1]^n \\ \mathcal{F}[u_2]^n \end{bmatrix} + \Delta t \begin{bmatrix} NL_1^n \\ NL_2^n \\ NL_3^n \end{bmatrix}. \quad (4.7)$$

Notice that, if the terms $\frac{\partial f}{\partial x_\alpha}$, for $f = w, u_1$ and u_2 , in M_α and $Q_{\alpha\beta}$, are regarded as $\frac{\partial f}{\partial x_\alpha} = \mathcal{F}^{-1}[ik_\alpha \mathcal{F}[f]]$, where $\mathcal{F}^{-1}[\cdot]$ represents the inverse Fourier transform, then, the

computation of the nonlinear terms involves only functions already obtained in the n -th time step. As a consequence, the 3×3 systems (4.7) with respect to the Fourier modes of different frequencies k_1 and k_2 in the $n+1$ -th time step are completely separated from each other, and thus can be solved independently. This much reduced the complexity of the discrete system, and of course the cost of the computation.

The numerical algorithm presented above is similar to that developed in [16, 17]. However, other than the difference in evolution equations, we notice that there is a significant difference in treating the stress terms. More precisely, in [16] the term $\hat{\sigma}_{\alpha\beta}^o \frac{\partial w}{\partial x_\beta}$ is treated as a linear term and implicitly discretized, while in the present paper, it is combined into the nonlinear term $\sigma_{\alpha\beta} \frac{\partial w}{\partial x_\beta}$ and explicitly discretized. We found in our numerical experiments that this leads to more stable long time evolution process in the numerical simulations. The reason for the improved stability might be explained by the fact that the term $\hat{\sigma}_{\alpha\beta}^o \frac{\partial w}{\partial x_\beta}$ is in fact an anti-diffusion term, thus if treated as a linear term, it will jeopardize the stability of the algorithm. However, for the total stress, especially in the neighborhood of the equilibrium, the effect will be much weakened.

5 Numerical results and discussions

In order to keep in accordance with the parameters in the experiments by Hobart [1], the thickness ratio h_r is fixed as $h_r = \frac{20}{3}$ with $H = 200$ nm and $h = 30$ nm in our numerical experiments, which are performed on a two dimensional computational cell with periodic boundary conditions. The dimensionless size of the computational cell is fixed as 1000×1000 , which turned out to be sufficiently large as compared with the effective wavelength involved in our numerical experiments. A fixed 128×128 uniform mesh is introduced on the computational cell, the corresponding Fourier space variables k_1 and k_2 are thus discretized accordingly and span respectively from $-\frac{128\pi}{1000}$ to $\frac{128\pi}{1000}$ with a step $\frac{2\pi}{1000}$. The time step Δt is fixed to 10 in our numerical experiments.

One of the characteristic quantity of a wrinkle pattern is its average wave number \bar{k} [16, 17], which is defined by

$$\bar{k}(t) = \sqrt{\frac{\sum |\hat{w}(m,n,t)|^2 k(m,n,t)^2}{\sum |\hat{w}(m,n,t)|^2}},$$

where $\hat{w}(m,n,t)$ is the intensity, with respect to the grid point (m,n) in the Fourier space at time t , of the Fourier transform of the out-of-plane displacement, $k(m,n,t)$ is the cor-

responding wave number, the summation is over all grid points (m,n) in the discrete Fourier space. The average wavelength L of a wrinkle pattern is given by

$$L(t) = \frac{2\pi}{\overline{k(t)}}.$$

The average deflection of a wrinkle pattern can be characterized by the root-mean-square (RMS) of the out-of-plane displacement w , namely

$$RMS = \sqrt{\frac{\sum w^2(m,n,t)}{N^2}},$$

where N^2 is the total number of the grid points.

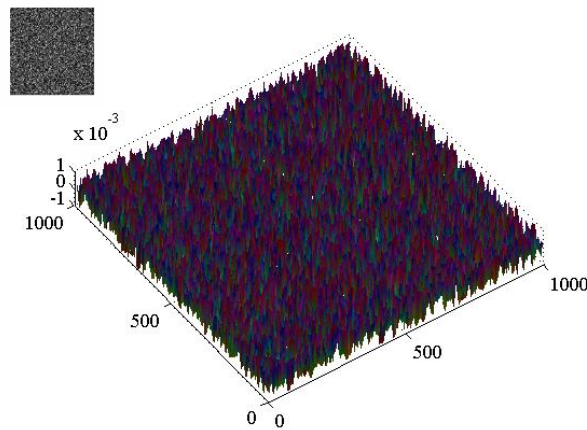


FIGURE 7: A typical initial random perturbation of the out-of-plane displacement with $RMS=0.000577$ and $L=19.2$. The upper inset shows the FFT spectrum of the wrinkle pattern.

Small random perturbations of amplitude 0.001 on the out-of-plane displacement of the flat film are taken as initial states in our numerical experiments, i.e. we set

$$u_1(x_1, x_2, 0) = u_2(x_1, x_2, 0) = 0, \text{ and } w(x_1, x_2, 0) = 0.001 \times \mathbf{Rand}(N^2),$$

where $\mathbf{Rand}(N^2)$ generates N^2 pseudo-random numbers with average distribution in $[-1, 1]$. As is shown by the top inset in Figure 7, the initial wrinkle pattern is generally completely disordered with its Fourier spectrum distributing randomly in the discretized Fourier space.

Figure 8 shows an evolution sequence of the simulated wrinkle pattern of the cubic crystal $Si_{0.7}Ge_{0.3}$ thin film on the viscous BPSG layer under an equi-biaxial compressive

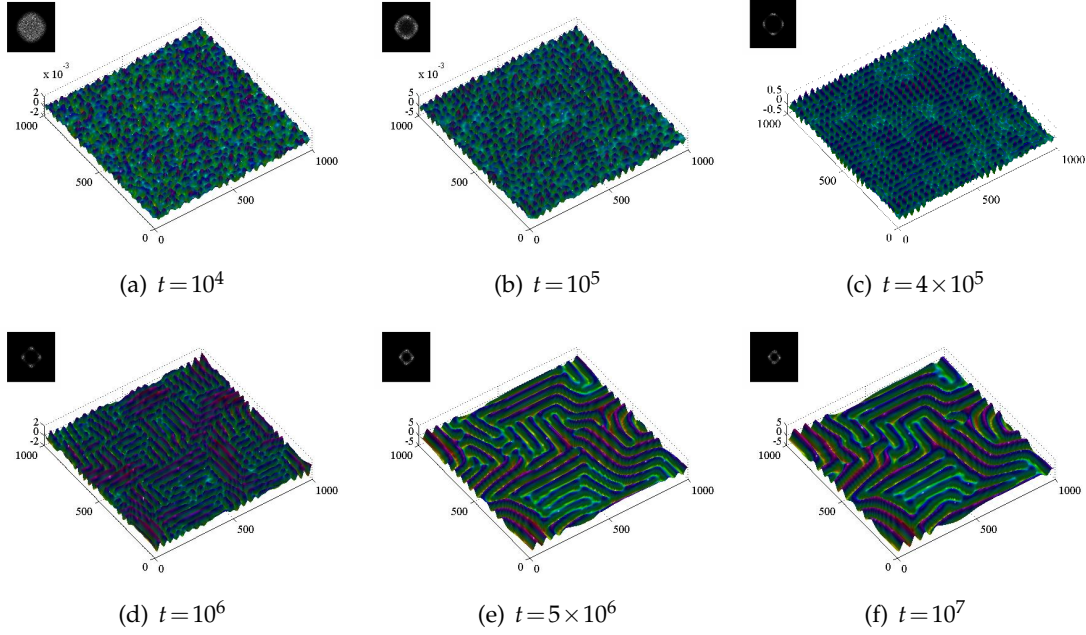


FIGURE 8: An evolution sequence of the wrinkle pattern for the cubic crystal $Si_{0.7}Ge_{0.3}$ film on a viscous layer under an equi-biaxial compressive residual stress with $\sigma_{11}^o = \sigma_{22}^o = -0.003C_{11}$. (a): $RMS = 0.000304$, $L = 40.7$; (b): $RMS = 0.000849$, $L = 40.1$; (c): $RMS = 0.121$, $L = 38.2$; (d): $RMS = 0.482$, $L = 44.3$; (e): $RMS = 0.868$, $L = 62.2$; (f): $RMS = 1.05$, $L = 71.8$.

residual stress with $\sigma_{11}^o = \sigma_{22}^o = -0.003C_{11}$. At $t = 10^4$, as is clearly seen from the top inset of Figure 8(a), the waves with wave numbers greater than a certain critical wave number \hat{k}_c have been obviously filtered out. This is consistent with the LSA, which predicts that the high frequency components with $k > k_c$ should decay exponentially while lower frequency components are unstable. This initial stage from $t = 0$ to $t = 10^4$ in our numerical experiments may be called filtering stage, which is generally very short and may hardly be observed in physical experiments, since the real perturbations generally do not have so much high frequencies in the first place. We notice that the average wavelength L increase dramatically from 19.2 to 40.7, while the average amplitude of the wrinkles RMS decreases only slightly from 0.000577 to 0.000304 in the filtering stage.

In the period roughly between $t = 10^4$ and $t = 10^5$, the average amplitude RMS begins to increase and the wave with the fastest growing wave number gradually dominates the wrinkle pattern (see Figure 8(b)). This process continues, and at $t = 4 \times 10^5$, the wrinkles self-assemble into a well-organized pattern, more precisely, there forms a bi-phase structure consisting of many island-like sub-structures each of which are locally aligned

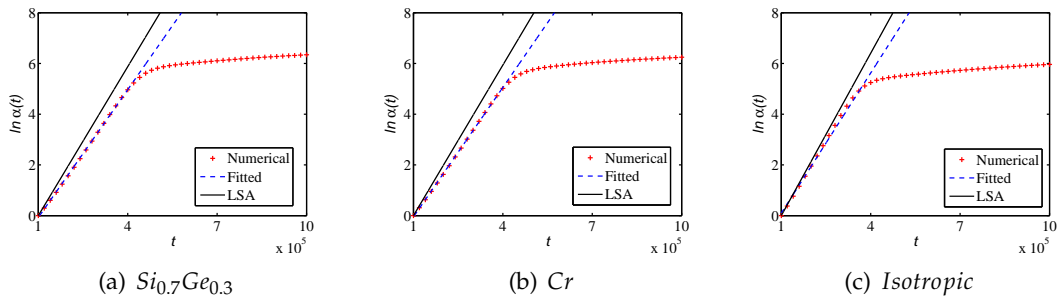


FIGURE 9: The amplitude of the wrinkles as a function of time at the latter part of initial growth stage for three different cubic crystals under an equi-biaxial compressive residual stress with $\sigma_{11}^o = \sigma_{22}^o = -0.003C_{11}$, where $\alpha(t)$ defined as the RMS at the time t normalized by the RMS at the time $t = 10^5$.

in either of the two orthogonal directions, [100] (the axis x_1 direction) and [010] (the axis x_2 direction) (see Figure 8(c)). The stage from $t = 10^4$ to $t = 4 \times 10^5$, may be named as the initial growth stage, which is characterized by slightly decreasing of the average wavelength L and exponentially fast growing of the average amplitude RMS. This stage can be well predicted by the LSA. In fact, the average wavelength L produced by the numerical experiment at the end of this stage is 38.2, which is very close to the fastest growing wavelength 37.5 along the [100] and [010] directions predicted by the LSA; and the growth rate of RMS, obtained by the least square data fitting of the numerical results, is 1.68×10^{-5} (see Figure 9(a)), which is also very close to the fastest growth rate 1.96×10^{-5} along the [100] and [010] directions predicted by the LSA. Numerical experiments as well as the LSA also show that the time span of the initial growth stage depends on the magnitude of the residual stress, the larger the residual stress the shorter the stage, and in general it is very short and hence can be difficult to capture sharply in physical experiments [3].

After the initial growth stage, the evolution process goes into the coarsening stage, which is characterized by the ever increasing wavelength and amplitude of the wrinkle pattern. As shown in Figure 8(d) through Figure 8(f), in this stage, the islands of bi-phase structure sprawl outwards, and the wrinkle pattern becomes coarser and coarser. The numerical results successfully reproduce the main features of the evolution process of the wrinkle pattern observed in the real experiments [1, 22–24].

The numerical simulations also reveal a uninterrupted coarsening dynamics with power law behavior. Figure 10 shows that, in the coarsening stage, the RMS and $L(t)$ can be well characterized by power laws of the form $RMS \propto t^\beta$ and $L(t) \propto t^\gamma$ respectively, where the exponents given by the least square data fitting are $\beta = 0.20$ and $\gamma = 0.17$. Con-

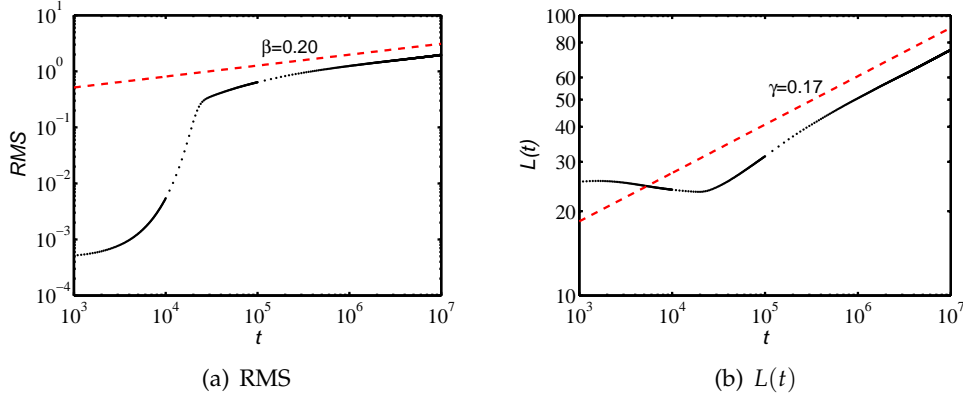


FIGURE 10: RMS and $L(t)$ as a function of t on a log-log plot for the coarsening dynamics of the wrinkle pattern for the cubic crystal $Si_{0.7}Ge_{0.3}$ film on a viscous layer under an equi-biaxial compressive residual stress with $\sigma_{11}^o = \sigma_{22}^o = -0.008C_{11}$. Results are from simulations averaged over ten random initial conditions.

Considering that the power law is independent of the materials degree of elastic anisotropy, this matches perfectly well with the result $L(t) \propto t^{\frac{1}{6}}$ for isotropic elastic films on incompressible thin viscous layers predicted by Im and Huang [16]. Figure 11 shows that the power law exponents are also independent of the magnitude of the residual stress.

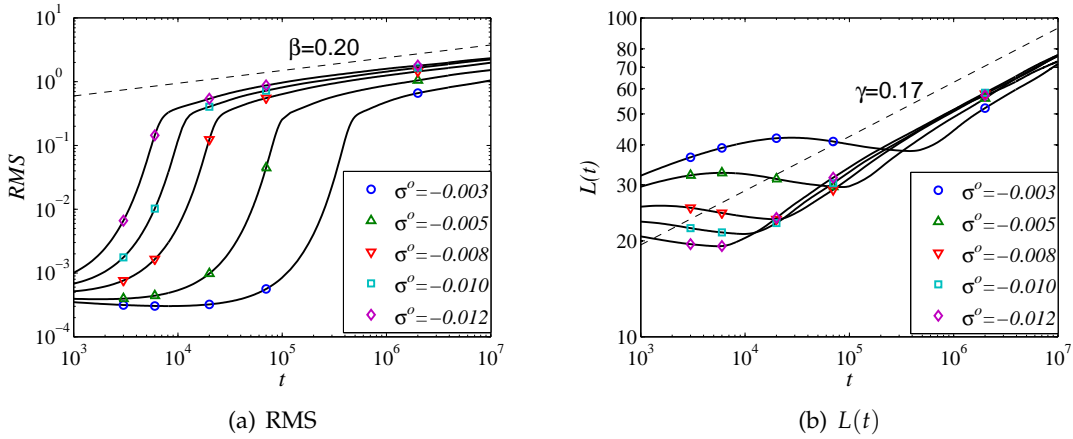


FIGURE 11: RMS and $L(t)$ as a function of t on a log-log plot for the coarsening dynamics of the wrinkle pattern for the cubic crystal $Si_{0.7}Ge_{0.3}$ film on a viscous layer under five different equi-biaxial compressive residual stresses.

Figure 12 shows an evolution sequence of the simulated wrinkle pattern for the cubic crystal Cr film under an equi-biaxial compressive residual stress with $\sigma_{11}^o = \sigma_{22}^o = -0.003C_{11}$. Similarly, the evolution process is clearly separated into three stages, i.e.

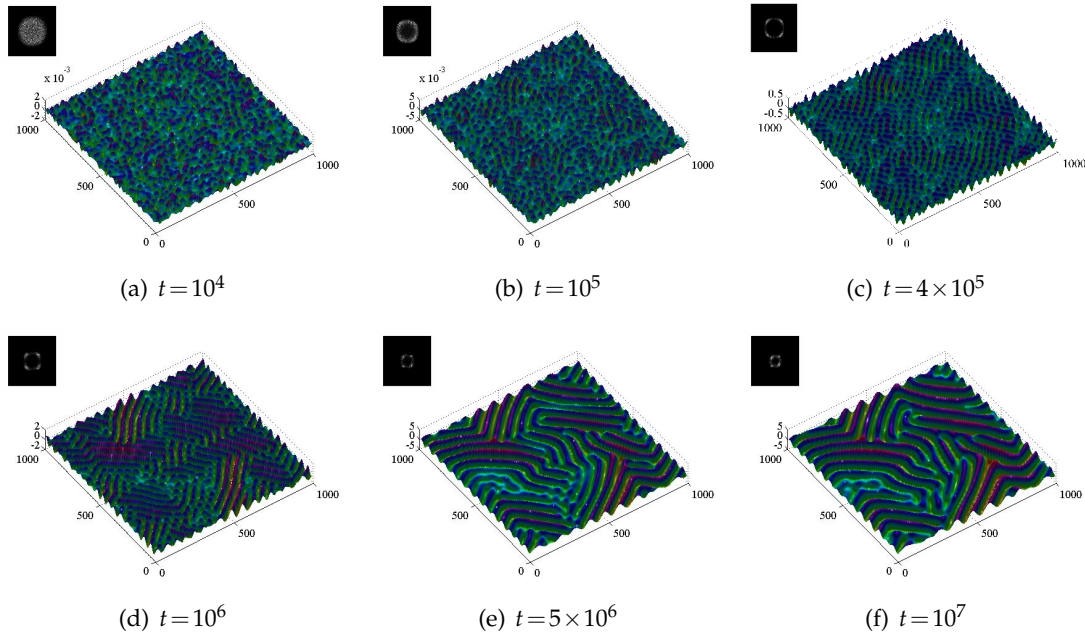


FIGURE 12: An evolution sequence of the wrinkle pattern for the cubic crystal Cr film on a viscous layer under an equi-biaxial compressive residual stress with $\sigma_{11}^0 = \sigma_{22}^0 = -0.003C_{11}$. (a): $RMS = 0.000310$, $L = 40.2$; (b): $RMS = 0.000930$, $L = 39.6$; (c): $RMS = 0.140$, $L = 38.0$; (d): $RMS = 0.480$, $L = 44.2$; (e): $RMS = 0.859$, $L = 62.1$; (f): $RMS = 1.03$, $L = 71.5$.

the filtering stage from $t = 0$ to $t = 10^4$ (Figure 12(a)), the initial growth stage as shown in Figure 12(b) through Figure 12(c), and the coarsening stage ($t \geq 10^6$) as shown in Figure 12(d) through Figure 12(f). We notice that, in this case, the bi-phase structure consists of island-like substructures locally aligned in the $[110]$ and $[\bar{1}10]$ directions ($\theta = \frac{\pi}{4}, \frac{3\pi}{4}$). This is consistent with the LSA performed in Section 3, since for the cubic crystal Cr the degree of elastic anisotropy is negative ($\zeta = -0.24$). The average wavelength $L = 38.0$ (see Figure 12(c)) at the end of the initial growth stage at about $t = 4 \times 10^5$ and the growth rate of $RMS = 1.70 \times 10^{-5}$ (see Figure 9(b)) during the initial growth stage produced by the numerical experiments are again very close to the corresponding values 37.3 and 1.98×10^{-5} predicted by the LSA.

Figure 13 shows an evolution sequence of the simulated wrinkle pattern for an isotropic elastic film (with elastic constants given by Table 1) on a viscous layer under an equi-biaxial compressive residual stress with $\sigma_{11}^0 = \sigma_{22}^0 = -0.003C_{11}$. Again, the evolution process is separated into the filtering stage from $t = 0$ to $t = 10^4$ (Figure 13(a)), the initial growth stage as shown in Figure 13(b) through Figure 13(c), and the coarsening stage

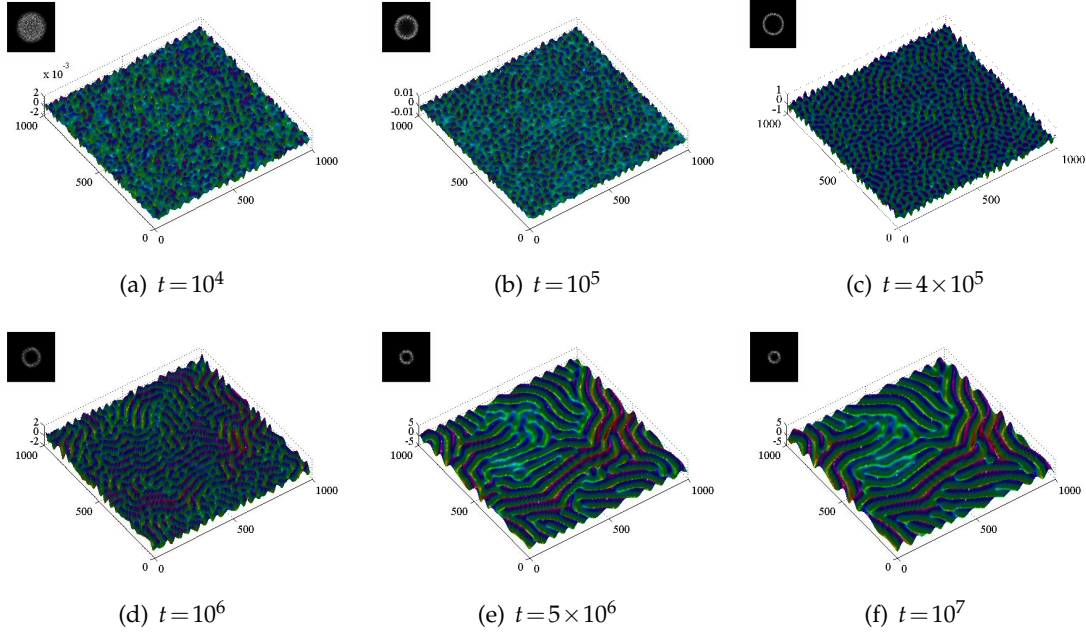


FIGURE 13: An evolution sequence of the wrinkle pattern for an isotropic elastic film on a viscous layer under an equi-biaxial compressive residual stress with $\sigma_{11}^0 = \sigma_{22}^0 = -0.003C_{11}$. (a): $RMS = 0.000329$, $L = 38.6$; (b): $RMS = 0.00134$, $L = 37.7$; (c): $RMS = 0.255$, $L = 37.4$; (d): $RMS = 0.522$, $L = 45.7$; (e): $RMS = 0.927$, $L = 64.3$; (f): $RMS = 1.09$, $L = 72.5$.

($t \geq 10^6$) as shown in Figure 13(d) through Figure 13(f). As clearly shown in Figure 13, the Fourier spectrum in the Fourier space always takes the form of a ring, in other words, there is no preferred directions for the wrinkles. This is of course a nice reflection of the material isotropy and is in perfect agreement with the LSA result obtained in Section 3. The numerical results, at $t = 4 \times 10^5$, of the average wavelength $L = 37.4$ (see Figure 13(c)) and the RMS growth rate 1.84×10^{-5} (see Figure 9(c)) are again very close to the fastest growing wavelength 36.6 and the fastest growth rate 2.14×10^{-5} predicted by LSA for the material in question. We notice here that the transition from an island-like pattern (Figure 13(c)) to a labyrinthine pattern (Figure 13(d)) produced by our numerical experiments is very similar to that observed in the physical experiments on certain stress-driven wrinkling [3].

6 Conclusions

A coupled temporal-spatial evolution PDEs system combining the FvK plate theory and the Reynolds lubrication theory is established to model the wrinkling evolution problem

of a cubic crystal elastic film on a viscous layer. By the LSA, it is shown that, during the initial growth stage, for materials with cubic crystalline symmetry, the sign of the degree of the elastic anisotropy $\zeta = \frac{C_{12}+2C_{44}}{C_{11}} - 1$ plays an important role in the anisotropy of the buckling instability of the thin film system. More precisely, the growth rate of the fastest growing wave number, taking as a function of directions, reaches a peak in the $\langle 100 \rangle$ directions for $\zeta > 0$, and in the $\langle 110 \rangle$ directions for $\zeta < 0$.

To explore the long time evolution behavior of the wrinkling pattern, a highly efficient semi-implicit spectral algorithm is developed. The numerical experiments show that the wrinkling evolution process can be separated into three main stages: the first is the filtering stage in which high frequency components are filtered out; the second is the initial growth stage in which the average wavelength drops slightly and the wrinkle amplitude grows exponentially; the third is the coarsening stage in which the amplitude as well as the average wavelength of the wrinkles increase constantly and exhibit a power law scaling. Moreover, numerical experiments show that the wrinkle pattern evolution at the initial growth stage can be well predicted by LSA. Numerical experiments for the coarsening stage also reproduce the main features of the pattern formation and evolution observed in physical experiments.

We notice that that it is possible to extend our method to the incompressible viscoelastic substrates, and to find equilibrium wrinkle patterns of elastic thin films on compliant substrates [2, 18–21, 33–35], which will be left for future studies.

Acknowledgments

We would like to thank anonymous referees for helpful comments. The research was supported by the Major State Basic Research Projects (2005CB321701), NSFC projects (10431050 and 10871011) and RFDP of China.

References

- [1] K.D. Hobart, F.J. Kub, M. Fatemi, M.E. Twigg, P.E. Thompson, T.S. Kuan and C.K. Inoki. Compliant substrates: a comparative study of the relaxation mechanisms of strained films bonded to high and low viscosity oxides, *J. Electron. Mater.*, 29:897, 2000.
- [2] N. Bowden, S. Brittain, A.G. Evans, J.W. Hutchinson and G.M. Whitesides. Spontaneous formation of ordered structures in thin films of metals supported on an elastomeric polymer, *Nature(London)*, 146:393, 1998.

- [3] P.J. Yoo and H.H. Lee. Evolution of a stress-driven pattern in thin bilayer films: spinodal wrinkling, *Phys. Rev. Lett.*, 91:154502, 2003.
- [4] J.S. Huang, M. Juskiewicz, W.H. de Jeu, E. Cerda, T. Emrick, N. Menon and T.P. Russell. Capillary wrinkling of floating thin polymer films, *Science*, 317:650, 2007.
- [5] C. Harrison, C.M. Stafford, W.H. Zhang and A. Karim. Sinusoidal phase grating created by a tunably buckled surface, *Appl. Phys. Lett.*, 85:4016, 2004.
- [6] W.T.S. Huck, N. Bowden, P. Onck, T. Pardoen, J.W. Hutchinson and G.M. Whitesides. Ordering of spontaneously formed buckles on planar surfaces, *Langmuir*, 16:3497, 2000.
- [7] S.P. Lacour, J. Jones, Z. Suo and S. Wagner. Design and performance of thin metal film interconnects for skin-like electronic circuits, *IEEE Electron Device Lett.*, 25:179, 2004.
- [8] C.M. Stafford, C. Harrison, K.L. Beers, A. Karmis, E.J. Amis, M.R. Vanlandingham, H.C. Kim, W. Volksen, R.D. Miller and E.E. Simonyi. A buckling-based metrology for measuring the elastic moduli of polymeric thin films, *Nature Mater.*, 3:545, 2004.
- [9] N. Sridhar, D.J. Srolovitz and Z. Suo. Kinetics of buckling of a compressed film on a viscous substrate, *Appl. Phys. Lett.*, 78:2482, 2001.
- [10] R. Huang and Z. Suo. Wrinkling of a compressed elastic film on a viscous layer, *J. Appl. Phys.*, 91(3):1135, 2002.
- [11] R. Huang and Z. Suo. Instability of a compressed elastic film on a viscous layer, *Int. J. Solids. Struct.*, 39(7):1791, 2002.
- [12] N. Sridhar, D.J. Srolovitz and B.N. Cox. Buckling and post-buckling kinetics of compressed thin films on viscous substrates, *Acta Mater.*, 50:2547, 2002.
- [13] J. Liang, R. Huang, H. Yin, J.C. Sturm, K.D. Hobart and Z. Suo. Relaxation of compressed elastic islands on a viscous layer, *Acta Mater.*, 50:2933, 2002.
- [14] S.H. Im and R. Huang. Ratcheting-induced wrinkling of an elastic film on a metal layer under cyclic temperatures, *Acta Mater.*, 52:3707, 2004.
- [15] S.H. Im and R. Huang. Evolution of wrinkles in elastic-viscoelastic bilayer thin film, *J. Appl. Mech.*, 72:955, 2005.
- [16] S.H. Im and R. Huang. Dynamics of wrinkle growth and coarsening in stressed thin films, *Phys. Rev. E*, 74:26214, 2006.
- [17] S.H. Im and R. Huang. Wrinkle patterns of anisotropic crystal films on viscoelastic substrates, *J. Mech. Phys. Solids*, 56:3315, 2008.
- [18] Z.Y. Huang, W. Hong and Z. Suo. Evolution of wrinkles in hard films on soft substrates, *Phys. Rev. E*, 70: 030601(R), 2004.
- [19] Z.Y. Huang, W. Hong and Z. Suo. Nonlinear analyses of wrinkles in a film bonded to a compliant substrate, *J. Mech. Phys. Solids*, 53:2101, 2005.
- [20] X. Chen and J.W. Hutchinson. A family of herringbone patterns in thin films, *Scripta materialia*, 50:797, 2003.
- [21] X. Chen and J.W. Hutchinson. Herringbone buckling patterns of compressed thin films on

- compliant substrates, *J. Appl. Mech.*, 71:597, 2004.
- [22] C.-Y. Yu, P.-W. Chen, S.-R. Jan, M.H. Miao, K.-F. Liao and C.W. Liu. Buckled SiGe layers by the oxidation of SiGe on viscous SiO_2 layers, *Appl. Phys. Lett.*, 86:011909, 2005.
- [23] R.L. Peterson, K.D. Hobart, F.J. Kub, H. Yin and J.C. Sturm. Reduced buckling in one dimension versus two dimensions of a compressively strained film on a compliant substrate, *Appl. Phys. Lett.*, 88:201913, 2006.
- [24] C.-Y. Yu, C.-J. Lee, C.-Y. Lee, J.-T. Lee, M.H. Miao and C.W. Liu. Buckling characteristics of SiGe layers on viscous oxide, *J. Appl. Phys.*, 100:063510, 2006.
- [25] Y.H. Lo. New approach to grow pseudomorphic structures over the critical thickness, *Appl. Phys. Lett.*, 59:2311, 1991.
- [26] J.E. Ayers. Compliant substrates for heteroepitaxial semiconductor devices: theory, experiment, and current directions, *J. Electron. Mater.*, 37:1511, 2008.
- [27] D. Landau and E.M. Lifshitz. *Theory of Elasticity*, London: Pergamon Press, 1959.
- [28] S. Timoshenko and S. Woinowsky-Krieger. *Theory of Plates and Shells*, 2nd edition, McGraw-Hill, New York, 1959.
- [29] W. Lu and Z. Suo. Symmetry breaking in self-assembled monolayers on solid surface. II. Anisotropic substrate elasticity, *Phys. Rev. B*, 65:205418, 2002.
- [30] L.B. Freund and S. Suresh. *Thin Film Material*, Cambridge: Cambridge University Press, 2003.
- [31] O. Reynolds. On the theory of lubrication and application to Mr. Beauchamp Tower's experiments including an experimental determination of the viscosity of olive oil, *Phil. Trans. Roy. Soc.(London)*, 177:157, 1886.
- [32] L.Q. Chen and J. Shen. Applications of semi-implicit Fourier-spectral method to phase field equations, *Comp. Phys. Comm.*, 108:147, 1998.
- [33] W.M. Choi, J. Song, D.-Y. Khang, H.Q. Jiang, Y. Huang and J.A. Rogers. Biaxially stretchable "wavy" silicon nanomembranes, *Nano Lett.*, 7:1655, 2007.
- [34] H.Q. Jiang, D.-Y. Khang, J. Song, Y. Sun, Y. Huang and J.A. Rogers. Finite deformation mechanics in buckled thin films on compliant supports, *Proc. Natl. Acad. Sci.*, 104:15607, 2007.
- [35] J. Song, H.Q. Jiang, W.M. Choi, D.-Y. Khang, Y. Huang and J.A. Rogers. An analytical study of two-dimensional buckling of thin films on compliant substrates, *J. Appl. Phys.*, 103:014303, 2008.